PHILOSOPHICAL TRANSACTIONS OF THE ROYAL SOCIETY A MATHEMATICAL, PHYSICAL & ENGINEERING SCIENCES

On the dilation of diamond by nitrogen impurity aggregated in A defects

The Royal Society

Phil. Trans. R. Soc. Lond. A 1998 **356**, 1397-1419
doi: 10.1098/rsta.1998.0227

The Royal Society

On the dilatation of diamond by nitrogen impurity aggregated in A defects

By A. R. Lang and G. Pang

H. H. Wills Physics Laboratory, University of Bristol, Tyndall Avenue, Bristol BS8 1TL, UK

Received 5 September 1996; accepted 5 December 1996

Contents

Lattice parameter measurements by modern methods of photography of transmitted divergent-beam X-ray diffraction patterns are reported. A small (less than 10 μm diameter) source of divergent CuKα X-rays is produced by an electron beam impinging on a thin copper film evaporated on to one surface of the diamond, which is placed in a scanning electron microscope. Patterns of high dispersion and high resolution are obtained by use of a 700 mm camera length and an Ilford L4 nuclear emulsion as the recording medium. A synthetic diamond volume containing only about one atomic part per 10^6 nitrogen impurity served as a pure-diamond standard. This was compared with a natural diamond of nearly pure IaA spectral type, unusually rich and uniform in content of nitrogen impurity aggregated in A-defect form (N concentration *ca.* 1135 atomic parts per 10^6). In both specimens, volumes free from dislocations and bounded by well-polished damage-free surfaces were probed. Advances in pattern-measuring methods included a film-stacking technique to improve signal-to-noise ratio, digitized microdensitometry and the measurement of pattern shifts relative to invariant datum points in the pattern provided by angularly sharp features arising from coherent multiple diffraction effects. Procedures were developed to correct for diffraction-line-profile asymmetry (which depends upon lattice perfection as well as other diffraction parameters). An absolute lattice parameter determination on the pure diamond yielded $a_0 = 0.356710(4)$ nm, considered to be a good value. After subtracting the calculated dilatation contribution (24%) due to a small population of {001} platelet defects in the nitrogen-rich diamond, the dilatation due to A defects

derived is $\Delta a_0/a_0 = (0.6 \pm 0.25) \times 10^{-6}[\mu_{\mathrm{A}(1282\ \mathrm{cm}^{-1})}/\mathrm{cm}^{-1}]$, where $\mu_{\mathrm{A}(1282\ \mathrm{cm}^{-1})}$ is the infrared absorption at $1282\,\mathrm{cm}^{-1}$ due to A defects, in units of cm^{-1}. In terms of $c_{\mathrm{N(A)}}$, the fractional atomic concentration in the diamond of nitrogen impurity present in A defects, and subject to more uncertainty, $\Delta a_0/a_0 = 0.036 c_{\mathrm{N(A)}}$, which indicates that a nitrogen atom in an A defect occupies *ca.* 1.11 times the volume of the normal carbon atom it replaces. This dilatation is compared with those expected from computed structures of the A defects.

Keywords: diamond lattice parameter; divergent-beam X-ray photography; Kossel patterns, X-ray; lattice parameter measurement; nitrogen in diamond; X-ray diffraction

1. Introduction

It was discovered by Kaiser & Bond (1959) that nitrogen was the principal impurity in most natural diamonds and was responsible for the ultraviolet and infrared absorptions that differentiate the majority (optical classification type Ia) from the rarer relatively pure ultraviolet-transmitting specimens (optical type II). They also found that nitrogen impurity increased the lattice constant, a_0, but did not change the physical density. It is now understood that nitrogen in diamonds can aggregate into small atomic clusters of several forms, distinguishable by characteristic ultraviolet and infrared absorptions (Davies 1977; Woods 1986; Evans *et al.* 1995). The simplest aggregate is the A centre, accepted as being a pair of nitrogen atoms substituting for a pair of carbon atoms on adjacent atomic sites in the diamond structure (Davies 1976). It is responsible for the A infrared absorption bands (principal peak at $1282\,\mathrm{cm}^{-1}$, 159 meV). Diamonds exhibiting the A absorption spectrum *only* are called type IaA; those exhibiting it dominantly form a significant fraction of the natural diamond population. The concentration of nitrogen impurity aggregated in A-centre form is customarily derived from the A-absorption strength by the relation $N_{\mathrm{A}} = Q_{\mathrm{A}}\mu_{\mathrm{A}}$, where N_{A} is the nitrogen concentration in atomic ppm, μ_{A} is the absorption coefficient (quoted in cm^{-1}) at wavenumber $1282\,\mathrm{cm}^{-1}$, and Q_{A} is a numerical coefficient. Kaiser & Bond found $Q_{\mathrm{A}} = 33$, a result accepted for many years. Recent nitrogen assays find much lower Q_{A} values: 17.5 ± 0.4 (Woods *et al.* 1990*a*), 16.2 ± 1 (Kiflawi *et al.* 1994) and 16.1 ± 1 (Boyd *et al.* 1994). (The last-named workers suggest taking $Q_{\mathrm{A}} = 16.5 \pm 1$, this being the weighted mean of their findings, those of Woods *et al.* (1990*a*) and of Kiflawi *et al.* (1994) combined.) This conflict between new and old Q_{A} values, and possible ways of resolving it, has been previously discussed (Lang 1993). Disregarding Kaiser & Bond's nitrogen assays but accepting their lattice dilatation and density measurements, and assuming that their specimens were purely type IaA in character, brings Q_{A} down to about 26, still much larger than the recent findings. A much-needed fresh determination of lattice parameter dependence upon A-centre concentration, taking advantage of modern abilities for assessing specimen homogeneity and analysing absorption spectra, is reported here.

In both natural and synthetic diamonds it is quite difficult to find specimen volumes over $1\,\mathrm{mm}^3$ that are not demonstrably inhomogeneous in impurity content. Lattice-parameter determination on specimens this size, or smaller, presents no major difficulties when employing a modern embodiment of Lonsdale's method of photography of the transmitted divergent-beam X-ray diffraction pattern (Lonsdale 1947).

In the new arrangement, the specimen is placed in a scanning electron microscope (SEM) and a source of divergent CuKα X-rays is produced by an electron beam, not more than about 10 μm in diameter, impinging on a 2 μm thick Cu film evaporated on to one surface of the diamond. (The divergent-beam pattern (Kossel pattern) produced by an X-ray source external to the crystal is conventionally termed a pseudo-Kossel pattern.) In the present experiments, it was essential to use specimens of high lattice perfection and free from surface damage. Unfortunately, such specimens give divergent-beam patterns described by Lonsdale as 'so fine and faint that they are either not visible or hardly show up at all against the background of general radiation'. With the new technique the problem of low visibility of perfect-crystal transmitted Kossel patterns still remains. However, experiments with perfect crystals have led to new observations of coherent multiple diffraction phenomena at Kossel line intersections (Lang & Pang 1995; Lang 1995). These diffraction effects impose angularly sharp markers on otherwise relatively diffuse diffraction patterns. They played a key role in the pattern-measurement procedure employed in the present work.

2. Specimens

A 0.7 mm thick slice of undoped synthetic diamond, overall size 5.0×3.5 mm^2, surfaces polished close to (110) and $(\bar{1}\bar{1}0)$, contained an unusually well-developed $(1\bar{1}0)$ growth sector. This specimen (known as E1/87) has been comprehensively studied by ultraviolet and infrared absorption probing, colouration mapping, birefringence and Schlieren micrography, cathodoluminescence, and single-crystal and double-crystal X-ray topography (Burns *et al.* 1990; Lang *et al.* 1991*b*; Lang & Meaden 1991; Lang 1994*a*). In the $(1\bar{1}0)$ growth sector, nitrogen was present in concentration of only about 1 ppm. This sector was used as a standard for a nitrogen-free perfect diamond. It was free from dislocations, surface damage and detectable impurity-zoning, on the evidence of birefringence, cathodoluminescence and X-ray topography. It contained an insignificant population of μm-sized inclusions. Within its overall outcrop area (*ca.* 1.6×0.7 mm^2, see growth-sector maps in Burns *et al.* (1990) and Lang *et al.* (1991*b*)), it had opposed outcrop areas of *ca.* 0.5×0.5 mm^2 on both (110) and $(\bar{1}\bar{1}0)$ that were sufficiently remote from stress-producing growth sector boundaries for the volume between them to qualify as a perfect, pure and strain-free crystal.

The nominally type IaA specimen (called A70) was a well-polished rectangular block, $2 \times 1 \times 1$ mm^3, long axis parallel to a cube direction (taken as [001]), with its 2×1 mm^2 facets parallel to {110}. It had some mechanical damage along its edges, particularly in the vicinity of its (001) and $(00\bar{1})$ end facets, but its central volume was free from cracks, inclusions, dislocations or other strain centres resolvable by birefringence and X-ray topography (Lang *et al.* 1996). Its A-centre content was high ($\mu_{\mathrm{A}} \sim 70$ cm^{-1}) and unusually homogeneous. Cathodoluminescence emission was uniform and of the deep blue hue characteristic of type IaA matrices. In the absence of any birefringence, cathodoluminescence or X-ray topographic evidence of impurity zoning, identification of any (111)-type growth facets within the specimen was not possible. This raised the possibility that the specimen might be a volume of non-faceted, 'cuboid' growth, an undesirability in view of association of submicroscopic non-diamond bodies with such material (Lang 1974). However, the sharp infrared absorption lines at 3107 and 1405 cm^{-1} ubiquitous (though often weak) in type Ia diamonds (Runciman & Carter 1971; Woods & Collins 1983) always show very strong-

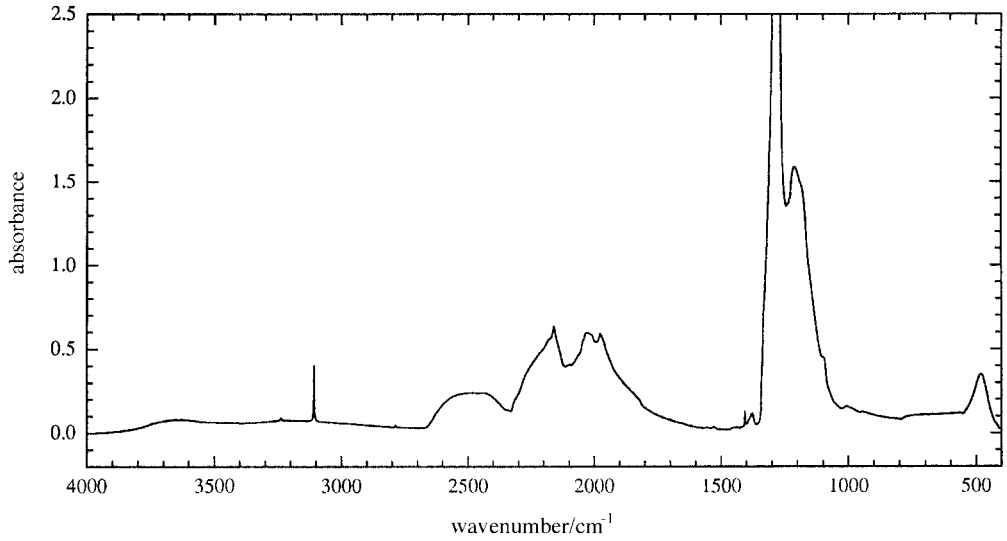

Figure 1. Infrared absorption spectrum of specimen A70. The absorption coefficient, μ_{A}, in the principal A-band absorption peak, at 1282 cm^{-1} (off scale), is derived from the absorption in the subsidiary A-band peak at 1212 cm^{-1}, as explained in text. Observe small and broad B′ peak at 1377 cm^{-1}. (Spectrum courtesy of Dr David Fisher.)

ly in cuboid growth material (Lang 1974; Welbourn *et al.* 1989). Fortunately, their strength in specimen A70 was no greater than that sometimes encountered in normal, {111}-faceted growth sectors in type Ia diamonds. Because of the high attenuation (*ca.* e^{-7}) at 1282 cm^{-1}, the value of μ_{A} was derived indirectly from the absorption at the subsidiary A-peak at 1212 cm^{-1} (150 meV), where it is just under half the value at 1282 cm^{-1} ($\mu_{\mathrm{A}(1282\ \mathrm{cm}^{-1})} = 2.03\mu_{\mathrm{A}(1212\ \mathrm{cm}^{-1})}$). The first infrared absorption spectra recorded of specimen A70 were regarded as examples of IaA type. Recent spectra taken with improved technique (for which the authors are greatly indebted to Dr David Fisher) require revision of that assessment. They have disclosed that the small and broad, B′, 'platelet' absorption (peaking at the unusually high frequency of 1377 cm^{-1}), though diminutive relative to the peak at 1282 cm^{-1} (see figure 1), has in absolute measure an integrated area, $I(\mathrm{B}')$, that cannot be ignored in its implications regarding both A-absorption measurement and the dilatation contribution by {001} platelet defects. The latter question is discussed in § 6. The former matter involves Woods's (1986) relation $\mu_{\mathrm{B}(1282\ \mathrm{cm}^{-1})}/\mathrm{cm}^{-1} = 20.5 \times 10^{-3} I(\mathrm{B}')/\ \mathrm{cm}^{-2}$, where $\mu_{\mathrm{B}(1282\ \mathrm{cm}^{-1})}$ is the strength of absorption by B-defects at 1282 cm^{-1}. Combining this relation with the known ratio of B-defect absorption at 1212 cm^{-1} to that at 1282 cm^{-1} (namely 1.5) indicates the correction to be made to the observed dominantly A-band spectrum to allow for a small B-defect-absorption component in the observed absorption at 1212 cm^{-1}. It corresponds to a reduction of 2.6% in A-band strength; and the resulting value of $\mu_{\mathrm{A}(1282\ \mathrm{cm}^{-1})}$ in the central volume of specimen A70 is 68.8 cm^{-1}, with an uncertainty that should be within ±2%. Combining this μ_{A} with the weighted value of Q_{A} recommended by Boyd *et al.* (1994), namely $Q_{\mathrm{A}} = 16.5 \pm 1$, indicates a nitrogen content in A-defect form of *ca.* 1135 atomic ppm in the region of specimen A70 probed in the lattice parameter measurement.

Specimens of pure IaA spectral type, exhibiting no detectable 'platelet' infrared absorption, do exist, but are very rare. Compensating for some departure from

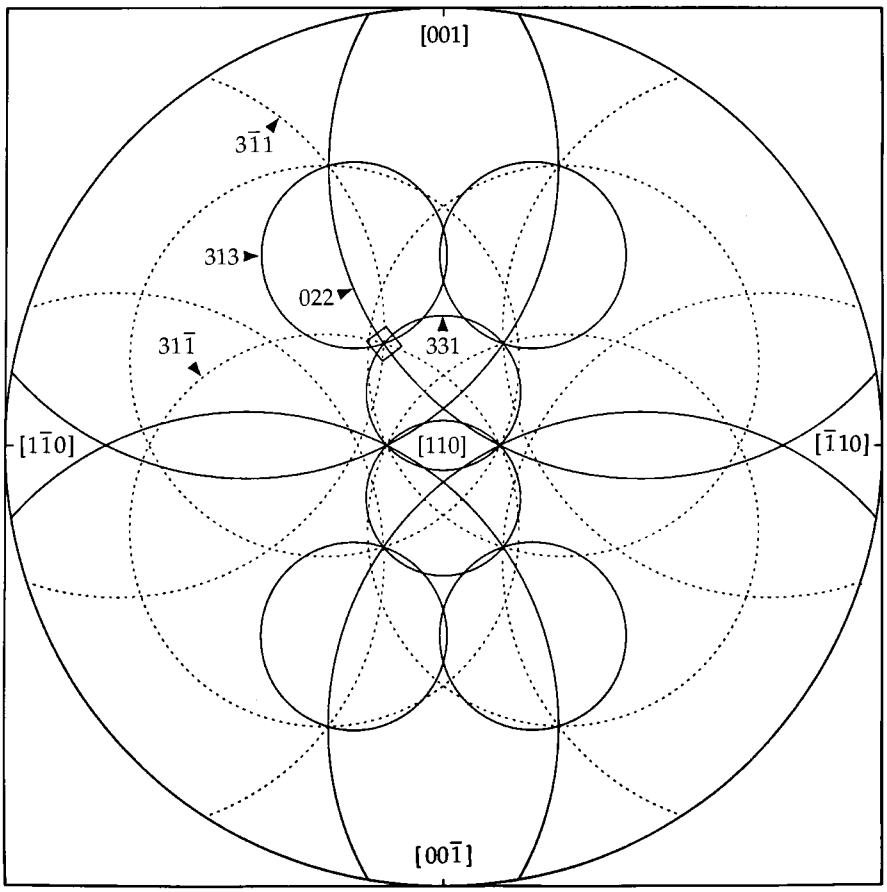

Figure 2. Stereographic projection on the X-ray exit surface, indexed (110), of Kossel cones of 220, 311 and 331 types that have intersections very close to the four symmetrically equivalent directions Q nearest to [110]. For clarity, the small circles of intermediate radii, representing 113-type cones, are distinguished by interrupted lines. The only cones indexed are those intersecting close to the Q direction $[11, 6, 6]$, which is rotated 2.38° from [211] towards [111]. Cone semi-angles, $90° - \theta_B$, apply to CuKα_1 radiation and the diamond lattice parameter, $a_0 = 0.3567$ nm. The Kossel patterns reproduced in figures 3, 4 and 5 include only a small fraction of the area of the small square surrounding $[11, 6, 6]$. The direction of the segment of the 022 circle crossing this square shows the orientations of figures 3, 4 and 5 relative to this projection.

this ideal in the case of specimen A70 was its demonstrated dislocation-free and birefringence-free central volume, coupled with an unusually high and uniform A-defect content.

3. Experimental arrangements

The general strategy used by Lonsdale (1947) was followed. It involves recording the transmitted divergent beam pattern in a direction Q, one of which is enclosed within the small square on the stereographic projection (figure 2). This Q, a member of the symmetrically equivalent four closest to [110], has direction $[11, 6, 6]$. Along that direction, when $\lambda/a_0 = 6/193^{1/2}$, the systematic intersection (i.e. an intersection

determined by lattice symmetry, independent of the ratio λ/a_0) of Kossel lines 331, $31\bar{1}$ and 022 (whose coplanar diffraction vectors lie in $(\bar{2}3\bar{3})$) coincides with that of its mirror image in $(01\bar{1})$, the systematic intersection of lines 313, $3\bar{1}1$ and 022, which have coplanar diffraction vectors lying in $(23\bar{3})$. (These intersections are illustrated in Lang & Pang (1995) and Lang (1995).) Of special concern is the (λ/a_0)-dependent, 'accidental' intersection of the 331 and 313 lines (always close to Q for diamond and CuKα_1 radiation) because their high Bragg angle, $\theta_B \sim 70°$, and acute crossing angle combine to produce a relatively large shift of the intersection point for a given Δa_0.

The principal pattern-recording experiments used a high-dispersion camera constructed by attaching a robust extension tube to the SEM chamber. This provided an evacuated specimen-to-film path of 700 mm. (An account of mechanical details associated with this camera is in preparation. Only essentials relevant to the diamond experiments are described here). The diamond specimens were themselves cemented to larger diamonds, polished blocks $5 \times 2 \times 1\ \mathrm{mm}^3$ in size. These blocks served to spread heat into a copper substrate, to reduce risk of specimen strain that could be caused by a direct specimen-to-copper bond, and to displace away from the line of sight from specimen through collimating aperture to film any more strongly scattering element than carbon. Under the copper substrate (a wedge-shaped block drilled to accommodate miniature thermistor temperature sensors) was a Peltier heating/cooling device for specimen temperature control. The Peltier device was supported by more massive copper members, which also provided a horizontal rotation axis for the specimen. With the help of this axis the desired specimen tilt was adjusted outside the SEM, using laser reflection from the specimen surface. Final minor adjustments were made in the SEM using its specimen orientation controls. The camera axis was inclined 15° downwards from the horizontal, avoiding need for the electron beam to impinge on the specimen's Cu-coated $(\bar{1}\bar{1}0)$ surface more obliquely than 45° to its normal. Standard operation of the SEM (a JEOL Type JSM 840) aided correct positioning of the electron beam impingement point, and the beam contamination mark revealed any broadening or wander that occurred during exposure.

Patterns were recorded on both Agfa–Gevaert Strukturix D3 double-coated X-ray film and on Ilford L4 nuclear plates, $50 \times 50\ \mathrm{mm}^2$ in area, emulsion thickness 25 μm. The former, being flexible, could be mounted on a Photoscan P-1000 digital drum scanner (Optronics International Inc.), which was extensively used for quantitative optical density measurement. The nuclear plates, developed grain size *ca.* 1 μm and emulsion thickness after processing *ca.* 10 μm, were preferred for photomicrography. With electron energy 30 kV and beam currents 7–10 μA, typical exposure doses were *ca.* 1200 μA minutes for specimen A70 (and about $\frac{2}{3}$ this for specimen E1/87) to achieve optical densities $D = \log_{10}(I_0/I_t)$ in the range 2.2–2.5 on either films or plates, after filtration by 15 μm-thick nickel foil.

4. Measurement procedures

Computer-generated Kossel patterns served indispensably as reference frames both when measuring pattern shifts visually and for defining position coordinates when summing and subsequently plotting digitized photometer scans of Kossel line profiles. Digitized photometry was performed on both the original Strukturix D3 films and on enlargements of L4 plates; manual work was done on enlargements only. An essential element in preparing enlargements of original X-ray films and plates was

the 'film stacking' procedure. For each specimen and each temperature setting several exposures were made. Selected plates were enlarged exactly four-fold on to Ilford Ortho sheet film to give images of density *ca.* 0.5 and moderate contrast. Several such films (three being the preferred number) each representing an independent experiment, were carefully superimposed to give a 'master' negative (resultant density *ca.* 1.5) from which could be obtained prints, such as figure 3, or by contact-printing on to another sheet film, an exact ×4 magnification of the original L4 plate but of lower mean density, say 0.8, suitable for manual measurement when placed over a standard viewing screen or for digitized densitometry by the drum scanner. Film stacking produced patterns with a much enhanced signal-to-noise ratio and diminished obtrusion by blemishes on individual plates. Precise stacking would not have been possible without the presence of the cross of sharp n-beam diffraction streaks of extra blackening resulting from enhanced Borrmann transmission at and near Q (see micrographs, figure 4). The average width of these streaks on the ×4 enlargements is under 100 μm, enabling the superimposed films to be correctly centred over each other within about 30 μm. For correct rotational setting, aligning the relatively sharp 022 Kossel lines was adequate.

The n-beam cross also served most valuably as a datum point, independent of specimen and temperature, from which to measure distance to the intersection of the 331 and 313 lines. (The centre of the n-beam cross was easily locatable on all the patterns recorded, the range of a_0 being small enough and the natural $K\alpha_1$ line-width large enough to ensure this.)

Measurement by visual line-fitting was the first procedure applied; the steps were as follows. Computed patterns of 331, 313 and 022 lines, with common intersection Q, were printed onto transparent overlays using fine red interrupted lines, on a scale to match exactly the ×4 film prints produced as described above. The 331 and 313 lines of the overlay were manually aligned with long segments of the 331 and 313 deficiency lines on the experimental patterns. For setting by eye, this was an ideal system: the weak red interrupted line provided colour contrast with the bluish-grey transmitted light of the deficiency line, and did not disturb its perceived intensity profile. (The 022 lines on the overlay served merely to check against rotational misalignment.) The principle is demonstrated in figure 5; but to illustrate it in monochrome, what in reality were weak red interrupted lines are here shown in high-contrast white. Distance x from the 331, 313 intersection to the centre of the n-beam cross was estimated to ±0.01 mm using a finely divided glass scale. The known film magnification, camera length and angular factors then give $\Delta a_0/a_0 = 3.55 \times 10^{-5}\Delta x$, taking x positive to the right in figure 5. Each pattern was measured twelve times by one experimenter (A.R.L.) and six times by the other (G.P.), with a shuffling of the six patterns (two specimens and three temperatures, nominally 20, 40 and 60 °C) between each cycle of measurements. The means $\bar{x}$ found by the two experimenters were in good agreement, and the standard deviations in each of the total of 18 measurements on each film did not exceed 0.12 mm, corresponding to deviations in a_0 of ±4 parts in 10^6. However, for both specimens, the values of a_0 found at '40 °C' and '60 °C' were considerably in excess of those expected from the thermal expansion coefficient of diamond (recommended value at 298 K, 1.00×10^{-6} deg^{-1} (Reeber & Wang 1996)). This prompted a post-mortem on the experimental set-up. The camera had been dismantled, but the specimen mounting assembly remained, still shrouded in Al foil and sheet against stray electron impact. Removal of this screening disclosed a blunder in the installation of the specimen-temperature-measuring thermistors, which had led to them

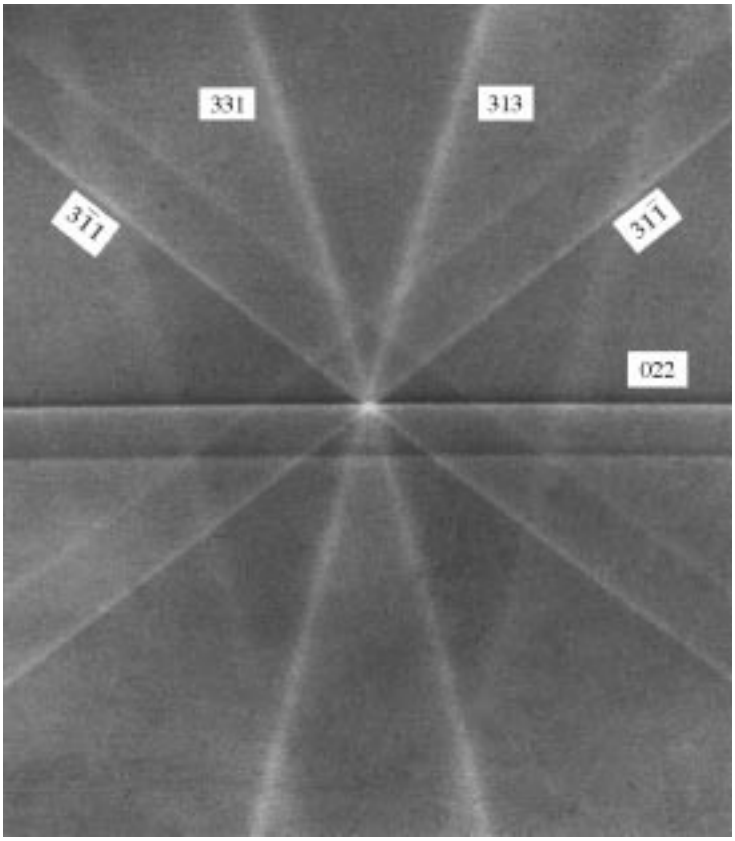

Figure 3. Divergent-beam pattern recorded from specimen A70 at room temperature, centred on the Q direction $[11, 6, 6]$. This is a positive print: light represents deficiency in transmitted intensity. The figure width subtends 1.5° at the specimen. Indexing of CuKα_1 lines corresponds with figure 2. Superimposed on the pronounced deficiency in the vicinity of Q resulting from incoherent addition of deficiency lines there stands out a six-armed cross of very fine dark lines representing enhanced transmission due to coherent multiple diffraction.

recording a temperature significantly lower than the true specimen temperature when the Peltier device was operated to raise the specimen temperature above ambient temperature deliberately. Consequently, lattice parameter measurements made at the elevated temperatures had to be discarded; they were of value only as indicators of good reproducibility and sensitivity of the measuring technique described above. Fortunately, the measurements at room temperature could be retained with confidence; it was unlikely that in these experiments the temperatures of specimens A70 and El/87 differed by more than one or two degrees. Direct conversion of the mean Δx value found in the room temperature experiments gave

$$[a_0(\mathrm{A70}) - a_0(\mathrm{E1/87})]/\bar{a}_0 = 5.86 \times 10^{-5}. \tag{4.1}$$

The principal measurement procedure employing digitized photometry was as follows. When the ×4 enlargements on film (such as used in the visual procedure described above) were scanned using a 50 µm × 50 µm pixel size, the n-beam cross was distinctly recorded. On expanded-scale computer displays of this region, coordinates of the cross-centre (i.e. point Q) could be reproducibly read within one-pixel limits. This pixel was then adopted as point Q in a computed reference pattern hav-

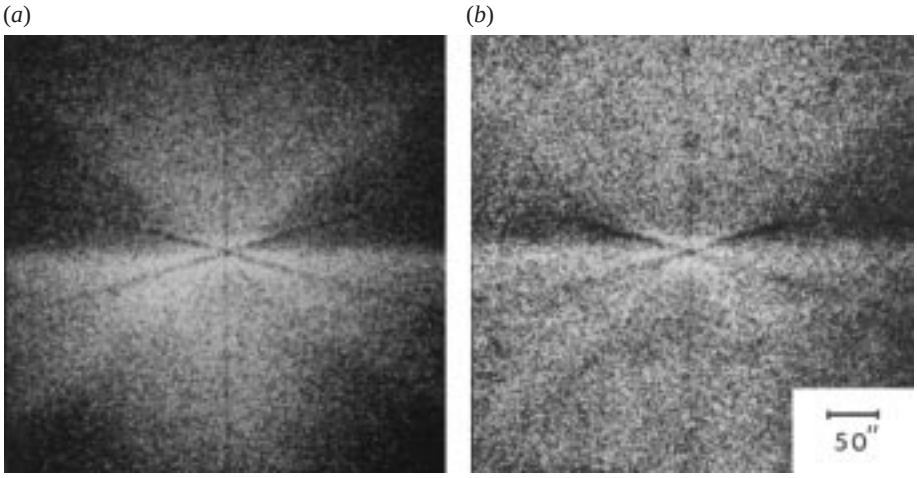

Figure 4. Micrographs of patterns close to Q showing the 'n-beam cross'. Orientation same as in figure 3. The $022\alpha_1$ line lies across the field at mid-height, the $022\alpha_2$ line runs below the bottom edge of the field. In the cross the dark line sloping from upper right to lower left results from coherent simultaneous diffraction by 022, 331 and $31\bar{1}$, and that sloping from upper left to lower right from coherent simultaneous diffraction by 022, 313 and $3\bar{1}1$. Coherent simultaneous diffraction within the 'accidental' intersection of 331 and 313 produces the sharp vertical dark line. At this magnification, the individual 331 and 313 deficiency lines are too broad and diffuse to be recognized, but the vertical dark line is about 50 times narrower. Patterns recorded at *ca.* 20 °C (*a*) by specimen E1/87 and (*b*) by specimen A70. Note sharper cross in (*a*), where on the original plates the width of the vertical line is 10–15 μm, equivalent to 3–4.5 arcseconds subtended at the specimen. Convolution of the X-ray source size, *ca.* 10 μm, with the angular range, say 1–2 arcseconds, of the minimally absorbed coherently simultaneously diffracted transmitted rays accounts for the observed line width satisfactorily.

ing the 022, 331 and 313 lines intersecting at Q. All the densitometered 331 and 313 line profiles pertaining to selected segments of these lines were then projected parallel to their respective computed reference lines to provide a mean measured profile. The displacement of the peak of this mean profile from the reference line (which corresponded to $\lambda/a_0 = 6/193^{1/2}$) could be measured easily. From the difference in displacement shown by specimens A70 and E1/87 their apparent difference in a_0 was obtained directly. On printouts of mean profiles, peak displacements were measured with an uncertainty of about ±0.05 minutes of arc in Bragg angle, corresponding to $\Delta a_0/a_0 = \pm 5 \times 10^{-6}$. The length of each selected Kossel line segment was about one third of the height of figure 3. For both 331 and 313, the data from two such lengths, centred, respectively, above and below the middle of figure 3 so as to avoid profile distortion by line crossing, were combined. The finding from this measurement procedure gave

$$[a_0(\mathrm{A70}) - a_0(\mathrm{E1/87})]/\bar{a}_0 = 6.32 \times 10^{-5}. \tag{4.2}$$

In a third procedure, single original D3 films were scanned. To keep noise low, the 50 μm × 50 μm pixel size was used. This provided ample resolution for recording the 331-type line profiles, sufficient for the 022 line, but insufficient for resolving the n-beam cross. Hence, in this case, recourse was had to setting the centre of the reference pattern at the intersection of the mirror plane with the 022 Kossel line, the subsequent geometrical analysis then being equivalent to that used by Lonsdale.

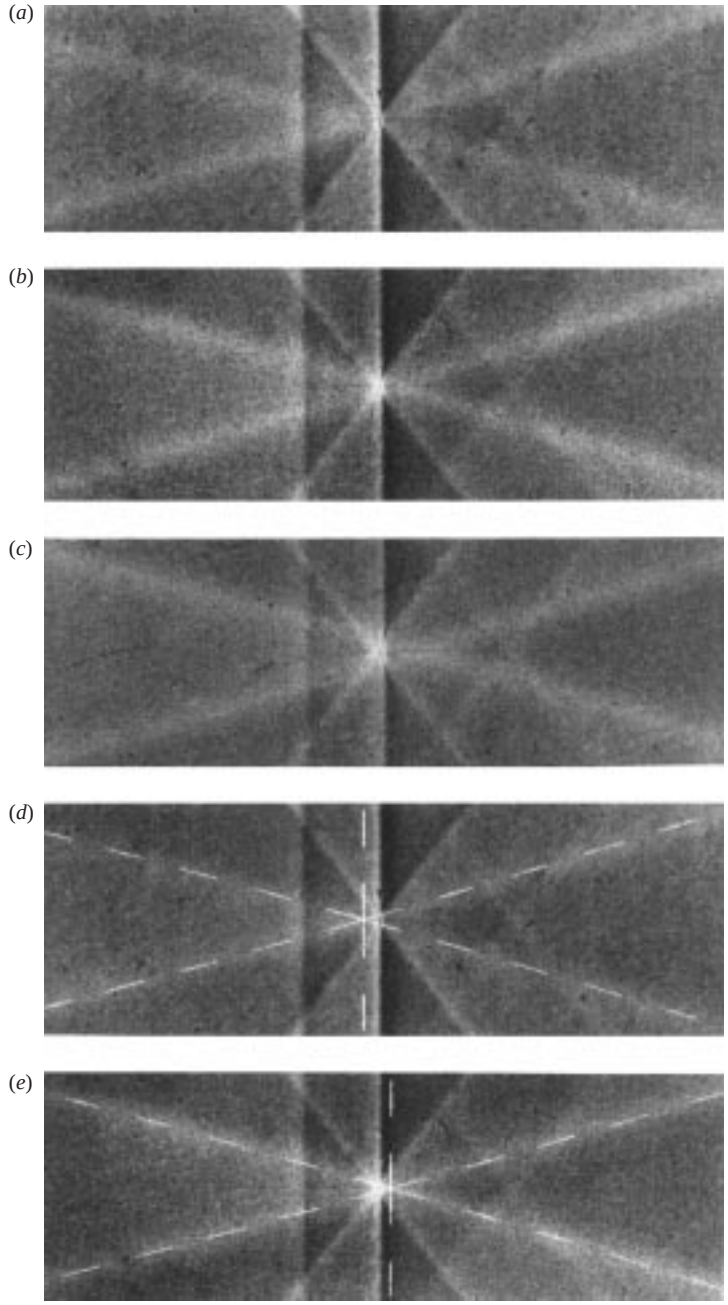

Figure 5. Movements of 331 and 313 deficiency line intersection point resulting from change of specimen and change of temperature. (Divergent-beam pattern rotated 90° clockwise relative to figure 3.) Positions of the 331 and 313 intersection point are measured from the cross centre as datum point: the intersection moves to the right as a_0 increases: (*a*) specimen E1/87, 20 °C; (*b*) specimen A70, 20 °C; (*c*) specimen A70, *ca.* 80 °C; (*d*) pattern (*a*) with pattern template superimposed; and (*e*) pattern (*b*) with template superimposed. (To clarify the illustration, the template displacement between (*d*) and (*e*) is shown somewhat larger than that given by the actual mean template settings.)

The finding was

$$[a_0(\mathrm{A70}) - a_0(\mathrm{E1/87})]/\bar{a}_0 = 5.93 \times 10^{-5}. \tag{4.3}$$

The much noisier line profiles resulting from use of only a single original X-ray exposure rendered this result significantly less reliable than those quoted in (4.1) and (4.2).

5. Deficiency-line profiles

In figures 2–5 the view is towards the X-ray exit surface, (110), and the signs of Kossel-cone indices are taken as those of the cone axes intersecting the near hemisphere in figure 2, following convention. However, in the case of higher-index cones whose axes are not far from [110], Bragg-case diffraction geometry applies at the $(\bar{1}\bar{1}0)$ surface; for these cones the diffraction vectors $\boldsymbol{g}$ and the diffracted waves (wave vector $\boldsymbol{K}_g$) make acute angles with $[\bar{1}\bar{1}0]$. Their incident waves (wave vector $\boldsymbol{K}_0$) are directed into the crystal, and after attenuation by extinction appear as deficiency lines in the transmitted divergent-beam pattern. (Although, as just explained, the active diffraction vectors in the case of these 311- and 331-type reflections have inverse indices to those shown on the figures, the index signs already applied to their deficiency lines will be retained, for convenience).

In early divergent-beam studies (well reviewed by Kossel (1937)), a marked intensity asymmetry in Kossel-line tails was observed, seen noticeably in Bragg-case geometry using rather perfect crystals. This 'hell-dunkel' effect (hereafter called HD for brevity) was explained by von Laue in his development of dynamical diffraction theory (see accounts by James (1954) and von Laue (1960)). All the lines seen in figure 3 display HD phenomena. They affect the profiles of the Bragg-case deficiency lines of immediate interest. Consequently, it was necessary to compare observed and computed profiles to establish what correction should be applied to the 'raw' measurements of Δa_0 quoted in § 4.

The physical factor dominating the strength of the HD effect is the magnitude of $\varepsilon\mu t$, where $\varepsilon = F''(hkl)/F''(0)$, the ratio of the imaginary part of the hkl structure factor to that for zero order, the latter being proportional to the normal linear absorption coefficient μ (which is 1.58 mm^{-1} for CuKα radiation in diamond). The specimen thickness is t (1 mm for A70 and 0.7 mm for E1/87). In the present case of high-angle diffraction, it is necessary to use the formulae and tabulations of Hildebrandt *et al.* (1975) to calculate ε. Included in ε is the Debye–Waller factor $\exp(-M)$, where $M = \mathrm{B}(\sin\theta_\mathrm{B}/\lambda)^2$. The experimentally found $\mathrm{B} = 0.142$ Å^2 (Takama *et al.* 1990) was adopted. (It differs insignificantly from $\mathrm{B} = 0.144$ Å^2 (Reid & Pirie 1980) used previously (Lang *et al.* 1991*a*).) The expressions of Hildebrandt *et al.* then give, for 331-type reflections from a perfect diamond, $\varepsilon = 0.642$ and $\varepsilon = 0.509$ for the σ and π polarization modes, respectively. Development of the HD effect is also sensitive to the inclination of Bragg planes and the plane of incidence to the X-ray entrance surface. In the present case, the planes of incidence do not contain the normal to the X-ray entrance surface, and the important geometrical factors concerned in determining positions of active wavepoints on the dispersion surface for a given angle of incidence are $\gamma_0' = \cos^{-1}(\boldsymbol{K}_0 \cdot \boldsymbol{q})$ and $\gamma_g' = \cos^{-1}(\boldsymbol{K}_g \cdot \boldsymbol{q})$, where $\boldsymbol{q}$ is a unit vector along the projection of [110] on the plane of incidence. (These factors differ slightly from those applying in the more familiar situation when the plane of incidence contains the normal to the entrance surface, in which case the corresponding

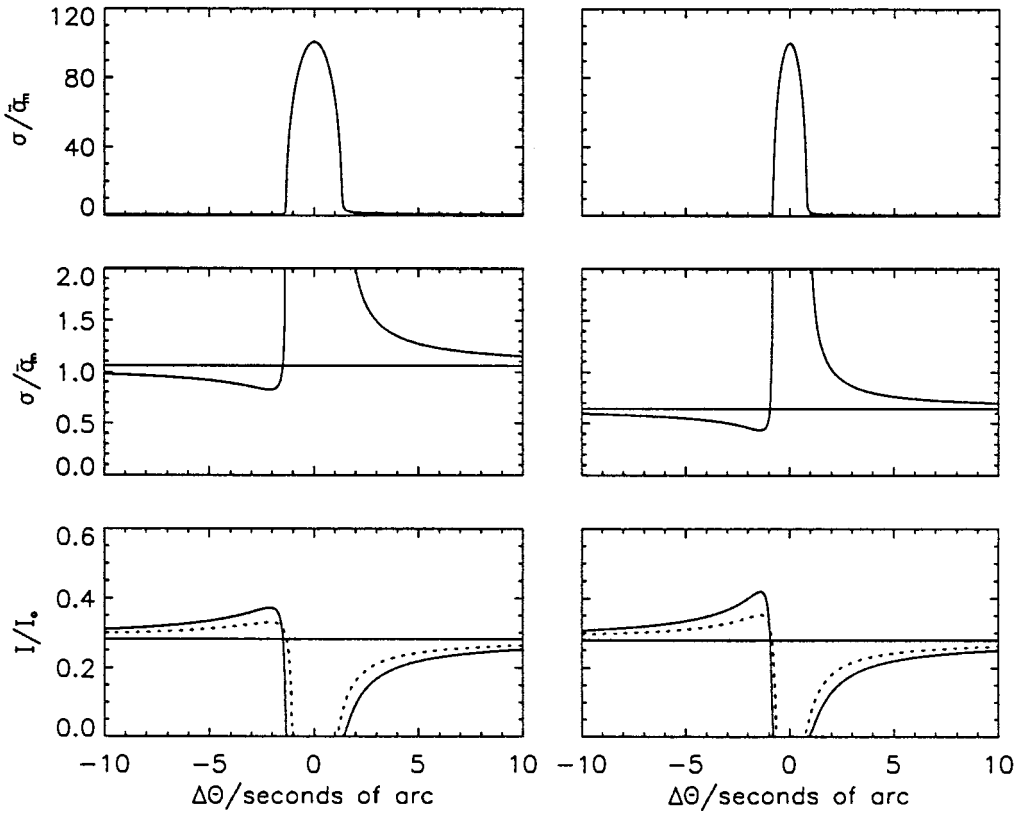

Figure 6. Extinction and HD asymmetry calculated for ideally monochromatic radiation, $\lambda = 0.154$ nm. Left column, reflection 331; right column, reflection 313. The angle $\Delta\theta$ is positive when the glancing angle, θ, exceeds that corresponding to zero deviation parameter, p. The top two rows show relative absorption (the unit of $\sigma/\bar{\sigma}_m$ is explained in the text). The calculations apply for $\varepsilon = 0.642$, $F(331) = 8.34$ and pure σ-mode polarized X-rays. The horizontal lines in the middle-row graphs indicate values of $\sigma/\bar{\sigma}_m$ remote from the deficiency line. The bottom row shows X-ray transmission when $t = 0.7$ mm, the horizontal lines corresponding to its value in absence of extinction and HD effects: continuous line, σ-mode polarization; interrupted line, π-mode polarization. For the latter polarization, the HD effect is less pronounced and the angular range of extinction is narrower (in the ratio $|\cos 2\theta|$:1).

factors are $\gamma_0 = \cos^{-1}(\boldsymbol{K}_0 \cdot \boldsymbol{n})$ and $\gamma_g = \cos^{-1}(\boldsymbol{K}_g \cdot \boldsymbol{n})$, where $\boldsymbol{n}$ is a unit vector along the inward-drawn normal to the X-ray entrance surface, i.e. $\boldsymbol{n}$ is parallel to [110] in the present case.) The strength of the HD effect and the angular range of strong extinction depend upon the ratio $|\gamma_g'/\gamma_0'|$, and hence differ for the 331 and 313 reflections. The exposition of dynamical diffraction theory by James (1963) provides expressions for calculating the effective absorption of K_0 waves within the range of strong extinction (i.e. of near total reflection from $(\bar{1}\bar{1}0)$) and at lower and higher Bragg angles. The results are plotted in figure 6, assuming ideally monochromatic radiation of CuKα_1-peak wavelength. The zero on the angle scale is the mid-point of the range of total reflection in the case of Bragg reflection from an infinitely thick, non-absorbing crystal. This is the range $-1 \leqslant p \leqslant 1$, where p is the deviation parameter (James 1963, equation (30.4)). The effective absorption coefficient, σ, which includes extinction, relates to penetration depth measured from $(\bar{1}\bar{1}0)$ (in the absence of Bragg reflection $\sigma = \mu/\gamma_0$). The unit of relative absorption plotted is the

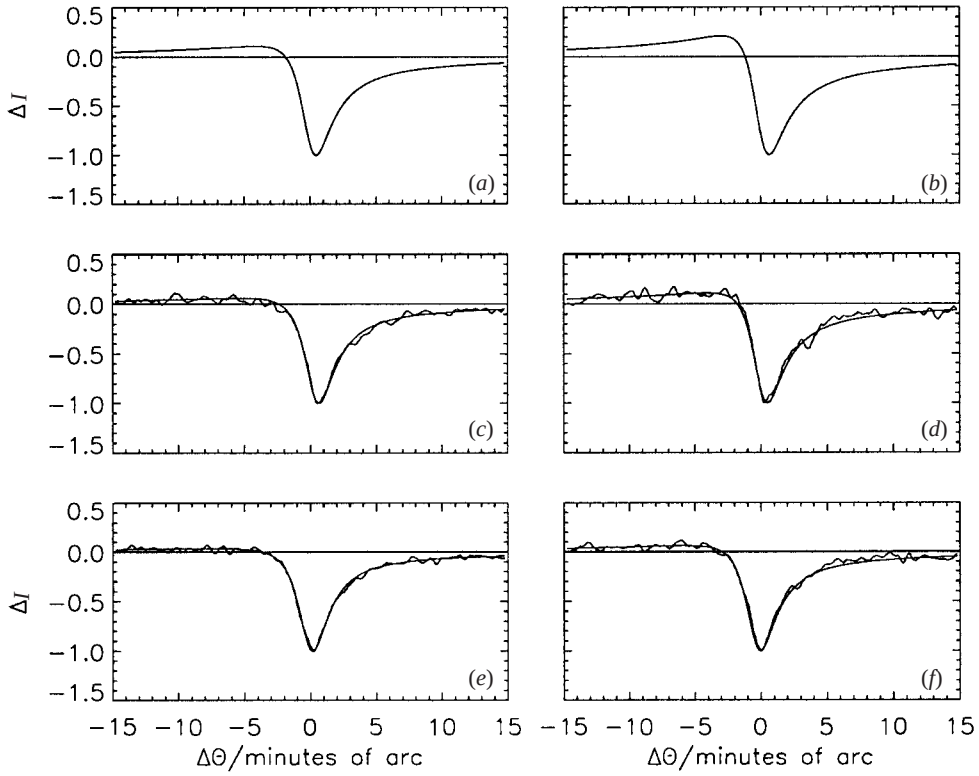

Figure 7. Deficiency-line profiles broadened by natural CuKα_1 wavelength spread. Comparison of observed and calculated profiles, unpolarized radiation. Left column reflection 331, right column 313. All curves normalized to $\Delta I/I = -1$ at peak deficiency. Computed curves (*a*) and (*b*): perfect crystal, $\varepsilon = 0.642$, $t = 0.7$ mm. Calculated peak $\Delta I/I = -1.57\%$ in (*a*), -1.15% in (b). Comparisons of digitally microdensitometered observed profiles with best-matching computed profiles for specimen E1/87, $\varepsilon = 0.45$, in (*c*) and (*d*), and for specimen A70, $\varepsilon = 0.30$, in (*e*) and (*f*). In (*c*)–(*f*), the observed peak percentage $\Delta I/I$ and (in parenthesis) calculated peak percentage $\Delta I/I$ are: (*c*) -1.01 (-1.62); (*d*) -0.67 (-1.20); (*e*) -1.22 (-1.84); (*f*) -1.18 (-1.39).

ratio $\sigma/\bar{\sigma}_m$, where $\bar{\sigma}_m = \mu/(\gamma_0|\gamma_g|)^{1/2}$. Its value outside the range $-1 \leqslant p \leqslant 1$ is too small to show on the top pair of graphs, but can be seen on the expanded scale used in the middle row. The resultant transmitted intensity, plotted in the bottom row in figure 6, applies for $t = 0.7$ mm only, but includes the case of π-mode polarization. The greater-than-normal transmission for $p > 1$ ($\Delta\theta$ negative), and the less than normal for $p < 1$ ($\Delta\theta$ positive), decay slowly to the normal value as $|p|$ increases.

In practice, the transmission curves of figure 6 must be convoluted with the angular profile due to wavelength spread in the CuKα_1 emission line. Recent measurements of its full width at half maximum intensity, $\Delta\lambda_{1/2}$, give $\Delta\lambda_{1/2}/\lambda = 2.85\times10^{-4}$ (Deutsch *et al.* 1995). This spreads the 331 and 313 lines angularly by 164 arcseconds and (with 700 mm camera length) linearly by 560 μm. Such spread, roughly 50 times the angular width of the high extinction range shown in figure 6, vastly reduces deficiency line contrast but enhances the relative importance of the extended wings of slightly abnormal absorption. The convolutions shown in figure 7, using the appropriate

Lorentzian for the CuKα_1 profile, average over both σ and π polarization modes and thus apply to the experimental conditions of unpolarized X-rays. The curves are all normalized to give $\Delta I = -1$ at the deficiency peak, the calculated percentage deficiencies (and those observed, where applicable) being given in the caption. As in figure 6, left and right columns refer, respectively, to the 331 and 313 reflections. The top two curves, (*a*) and (*b*), apply to an ideally perfect crystal, $\varepsilon = 0.642$, with $t = 0.7$ mm. The calculated profiles assume no radiation present other than CuKα_1 produced at the point of electron-beam impingement. This ignores contributions to film density from the white-radiation background in the X-ray emission spectrum, Compton scattering by the specimen and any radiation scattered by sources other than the specimen. In these circumstances, the relatively high ratio of $(\Delta I/I)_{\mathrm{obs}}$ to $(\Delta I/I)_{\mathrm{calc}}$ in the matched profiles indicates satisfactory experimental conditions.

Considerable effort was expended in finding the ε value that best fitted the line profiles obtained by digitized densitometry of the D3 films. By scan repetition to average out electronic noise, and by summing scans over 6 mm-long segments of the deficiency lines to average out film noise, the resultant noise level was brought down to the extent that few noise peaks seen in figure 7 correspond to $|\Delta I|/I > \frac{1}{1500}$. Most films showed some long-range non-uniformity of background, for reasons never established, and hence never eliminated experimentally. To produce the records shown in figure 7, the background was levelled by computer so as to match the calculated deficiency curves at the largest values of $|\Delta\theta|$ plotted. This left ε-matching to be decided by asymmetry genuinely present in the Kossel-line tails, as it should be. Best fits were, for both 331 and 313 reflections, $\varepsilon = 0.45$ for specimen E1/87 and $\varepsilon = 0.3$ for specimen A70, with an uncertainty judged to be less than 0.05 in ε. Table 1 shows the calculated peak shifts resulting from ε values covering the range from perfect crystal down to the level exhibited by A70. Asymmetry increases the apparent Bragg angle; asymmetry uncorrected would lead to a_0 values too low being adduced. In the present case, the differences in corrections applicable to each crystal give the corrections to be applied to $[\theta_{\mathrm{B}}(\mathrm{E1/87}) - \theta_{\mathrm{B}}(\mathrm{A70})]$, these being, in arcminutes, $-(0.309 - 0.260) = -0.049$ for 331 and $-(0.421 - 0.345) = -0.076$ for 313. The net pattern shift depends upon the mean of these, -0.062 arcminutes. This reduction of $[\theta_{\mathrm{B}}(\mathrm{E1/87}) - \theta_{\mathrm{B}}(\mathrm{A70})]$ reduces $[a_0(\mathrm{A70}) - a_0(\mathrm{E1/87})]/\bar{a}_0$ by 0.65×10^{-5}, and is in principle applicable equally to findings (4.1), (4.2) and (4.3).

6. Discussion

(*a*) *Measurement of lattice parameter difference*

As reported in § 4, the uncertainty in judging positions of peaks of the 331 and 313 deficiency lines was about 0.04 to 0.05 arcminutes, either when using the *n*-beam cross as datum (in the visual measuring method) or when measuring from computed Kossel lines intersecting at the cross (in the densitometric method); the uncertainty in a_0 resulting from this cause is thus about four to five parts per 10^6. Hence the uncertainty in measuring the difference between 331-type peak positions on two generally similar patterns by either method produces an uncertainty in lattice-parameter difference assessment of not more than about one part in 10^5. Uncertainty in magnitude of the correction needed to remove systematic error due to differences in line profile asymmetry depends on uncertainty in the difference in ε between the two specimens. If there were error in the ε values derived from observed Kossel line profiles (the method here used), then it would probably be either an over-assessment or

Table 1. *Calculated displacements of deficiency-line peaks from the angles corresponding to zero deviation parameter, due to the HD effect*

(Values of $\Delta\theta$/arcminutes that need to be subtracted from observed deficiency-peak glancing angles θ, listed according to reflection, specimen thickness and value of ε.)

	$t = 0.7$ mm (331)	$t = 1.0$ mm (331)	$t = 0.7$ mm (313)	$t = 1.0$ mm (313)
ε	$\Delta\theta$	$\Delta\theta$	$\Delta\theta$	$\Delta\theta$
0.30	0.204	0.260	0.276	0.345
0.40	0.274	0.350	0.372	0.467
0.45	0.309	0.395	0.421	0.532
0.55	0.382	0.492	0.525	0.669
0.65	0.461	0.596	0.637	0.820

an under-assessment in the case of both crystals, which would have a relatively small effect on the asymmetry correction difference, as figures in table 1 show. Specimen E1/87 exhibited excellent visibility of Pendellösung fringes and of images of dislocations (a few dislocations being present in other growth sectors), very similar to that manifested in a natural diamond whose ε value for reflection 220 was derived by double-crystal rocking curve profile analysis, using symmetrical transmission geometry for this reflection. The value then found, 0.69, was 0.72 times the theoretically expected value, 0.98 (Lang *et al.* 1991*a*). The finding $\varepsilon = 0.45$ for E1/87, 0.70 times the theoretical value, 0.642, is very plausible. Specimen A70 has lower perfection than E1/87, as comparison of X-ray topographic images given by the two specimens shows (Lang 1994*a*; Lang *et al.* 1996), and as is displayed here directly in the greater line breadth in the arms of its n-beam cross (figure 4). Taking $\varepsilon = 0.3$ for A70 is deemed a satisfactory choice on the evidence available. It follows that uncertainty in the asymmetry correction needed in the present experiments is not greater than ± 0.05 arcminutes; but this is still comparable with the full correction indicated by table 1, -0.062 arcminutes, which will now be applied. Combining the uncertainties discussed above suggests that possible error in the present lattice parameter difference measurement is about $\pm 1\frac{1}{2}$ parts in 10^5. This is large compared with differences between findings from the three measurement procedures employed. The values of $[a_0(\mathrm{A70}) - a_0(\mathrm{E1/87})]/\bar{a}_0$ quoted in (4.1), (4.2) and (4.3) become, after correction, 5.21, 5.67 and 5.28×10^{-5}, respectively. There is no strong reason for giving different weights to (4.1) and (4.2), but both are more reliable than (4.3). Accordingly, (4.1), (4.2) and (4.3) are given weights of 1, 1 and 0.5, respectively, yielding, with the fairly cautious error estimate proposed,

$$[a_0(\mathrm{A70}) - a_0(\mathrm{E1/87})]/\bar{a}_0 = (5.41 \pm 1.5) \times 10^{-5}. \tag{6.1}$$

(*b*) *Lattice parameter of pure diamond*

For the lattice parameter measurements reported here, and for others recently reported (Holloway *et al.* 1991, 1992) or discussed (Lang 1994*b*), the CuKα_1 peak wavelength is taken to be 0.15405945 nm (Cohen & Taylor 1986). (The difference from the more recent Jena value (Härtwig *et al.* 1991), which is one part in 10^6 smaller, is not significant in the accuracy range under consideration.) For specimen E1/87, the difference, $\Delta\theta$, between the observed mean 331 and 313 peak Bragg angle and

that of the reference pattern in which these lines intersect at the n-beam cross, and relative to which measurements were made, was found to be $\Delta\theta = 0.419$ arcminutes by the visual measurement method and $\Delta\theta = 0.475$ arcminutes by the densitometric method. From the mean of these values must be subtracted the asymmetry correction appropriate to E1/87, 0.365 arcminutes, giving $\Delta\theta = 0.082$ arcminutes for the condition $p = 0$, and hence a lattice parameter 0.3×10^{-5} nm smaller than that represented by the reference pattern.

Now when $p = 0$, Bragg's Law is satisfied exactly in the crystal by X-rays whose wavelength, λ_{cryst}, is related to that in vacuum, λ_{vac}, by the refractive-index relation $\lambda_{\mathrm{cryst}} = \lambda_{\mathrm{vac}}(1 + \delta)$, where $\delta = 1.126 \times 10^{-5}$ for diamond and CuKα radiation. If λ_{cryst} were also the wavelength of X-rays forming the n-beam cross, then the lattice parameter of E1/87 would be $[(193^{1/2}/6)\lambda_{\mathrm{cryst}} - 0.3 \times 10^{-5}]$ nm $= [(2.315407 \times 0.1540612) - 0.3 \times 10^{-5}]$ nm $= 0.3567114$ nm (the last digit here is retained only for comparison with what follows). However, the arms of the n-beam cross used for defining the centre of the reference pattern arise from coherent simultaneous 022-, 311- and 331-type reflections, and are formed by rays undergoing minimum absorption. Hence their wavelength lies between λ_{cryst} and λ_{vac}. To find the difference from λ_{cryst} requires a complex calculation, but some bounds can be put on the decrease in δ involved. For example, consider the two beam case, 022 reflection only, σ-mode polarization, with the simple geometry of symmetrical reflection or symmetrical transmission. Then for the least absorbed rays δ has the value δ_{min} given by $\delta_{\mathrm{min}} = [1 - (F(022)/F(0))]\delta = 0.68\delta = 0.77 \times 10^{-5}$. In the corresponding situation for the 311 reflection alone, $\delta_{\mathrm{min}} = [1 - (F(311)/F(0))]\delta = 0.81\delta = 0.91 \times 10^{-5}$, taking $F(022) = 15.39$ and $F(311) = 9.07$. In a three beam case involving both these reflections in the same hypothetical diffraction geometry, a lower bound on δ_{min} would be $\delta_{\mathrm{min}} = \{1 - [(F(022) + F(311))/F(0)]\}\delta = 0.49\delta = 0.56 \times 10^{-5}$. With the complex three-dimensional geometry involved in the present case, reduction of δ as great as that represented in the last figure is not likely, despite addition of another simultaneous reflection (that of 331 type). For present purposes, the rather arbitrary assumption will be made that the cross arms in question are produced by the wavelength $\lambda_{\mathrm{cross}} = \lambda_{\mathrm{vac}}(1 + 0.65\delta)$, with an uncertainty of about ± 0.1 in the fraction multiplying δ, and hence of about ± 1 part per 10^6 in the wavelength producing the reference Kossel pattern. The resulting value of a_0, slightly reduced compared with that derived above, is $a_0 = 0.3567099$ nm. Summing the various uncertainties involved indicates possible error of about ± 1 part in 10^5, and the experimental results can be stated as, for pure perfect diamond at room temperature (*ca.* 20 °C),

$$a_0 = 0.356710(4) \text{ nm}. \tag{6.2}$$

The result (6.2) may be compared with two other lattice parameter measurements on diamonds known from their infrared absorption spectra to have nitrogen impurity concentrations of $\leqslant 1$ ppm. The first comes from the original plot of a_0 versus absorption at 1282 cm^{-1} presented by Kaiser & Bond (1959), after converting to the present CuKα_1 wavelength value and making a refraction correction apparently omitted by those authors (Lang 1994*b*). Applying the refraction correction believed most appropriate in their experiments, Kaiser & Bond's value of a_0 becomes 0.356710 nm. The second measurement, using a double-crystal diffractometric technique (Holloway *et al.* 1991, 1992), found $a_0 = 0.356713(5)$ nm at 25 °C for synthetic, nitrogen-free diamonds containing carbon isotopes in the natural abundance ratio, but, on the evidence of their double-crystal rocking-curve widths, less strain free than E1/87. These published findings are compatible with the figure in (6.2).

(*c*) *Dilatation by A defects*

It is not permissible to proceed directly from (6.1) to calculate the dilatation produced by A defects. As described in § 2, the refined infrared absorption spectra taken by Dr David Fisher reveal that the {001} platelet defect population is sufficiently large to require its contribution to the observed dilatation to be taken into account. The principal quantities involved in estimating this contribution are: (a) the total platelet area per unit volume of crystal; and (b) the matrix displacement perpendicular to the platelet plane produced by the abnormal platelet cells, which have unit cell height greater than diamond a_0. Quantity (a) is derived by combining the observed $I(\mathrm{B}')$, $30.1 \pm 0.5\ \mathrm{cm}^{-2}$, with the relation $A_\mathrm{p}/\ \mu\mathrm{m}^{-1} = (9.0 \pm 2.1) \times 10^{-3} I(\mathrm{B}')/\mathrm{cm}^{-2}$ found by Sumida & Lang (1988), where A_p is the platelet area per unit volume, expressed as $\mu\mathrm{m}^2$ per $\mu\mathrm{m}^3$, and $I(\mathrm{B}')$ is expressed in reciprocal centimetres squared. This gives $A_\mathrm{p} = 0.271\ \mu\mathrm{m}^2/\ \mu\mathrm{m}^3$ in specimen A70, subject to the uncertainties stated. For (b), the abnormal platelet cell height, a_p, is taken as $(1.40 \pm 0.01)a_0$, adopting the value recently derived by Cherns *et al.* (1997), using convergent-beam electron diffraction, as being more accurate than that derived from electron microscope moiré patterns, $a_\mathrm{p} = 1.356 a_0$ (Bursill *et al.* 1981). Combining (a) with (b) gives $(a_\mathrm{p} - a_0)A_\mathrm{p}$, the increase in volume per $\mu\mathrm{m}^3$ arising from replacement of normal diamond FCC cells by platelet cells; the relative volume change $[\Delta V/V]_\mathrm{p}$ is 3.86×10^{-5}, with uncertainty of about $\pm 25\%$. Another quantity of interest is the average platelet diameter. The large width of the platelet peak in specimen A70, FWHM *ca.* $18\ \mathrm{cm}^{-1}$, and high peak wavenumber, $1377\ \mathrm{cm}^{-1}$, places these platelets at the top end of the plot of peak wavenumbers versus B′ peak FWHM in figure 2 of Woods (1986). This position characterizes the platelets in A70 as having unusually small diameters. How small could only be discovered by destructive thinning for TEM observation, but an estimate can be made. Curves plotted by Clackson *et al.* (1990) show how the B′ peak wavenumber moves upwards as platelet diameter decreases. Although platelet diameters and the B′ peak wavenumber that were measured on the same thinned specimen by Sumida & Lang fall below the curves of Clackson *et al.*, the trend of their curves can be applied to estimate the ratio of platelet sizes in A70 to those in the Sumida & Lang specimen, and to conclude thereby that the former is smaller by about a factor of two. Assuming similar size spreads, this makes the mean diameter of platelets in A70 about 9 nm and their mean area $80\ \mathrm{nm}^2$, very roughly. Combining this with the value of A_p derived, yields a number density of *ca.* 3.4×10^3 platelets per $\mu\mathrm{m}^3$, and corresponding mean interplatelet distance *ca.* 67 nm, very much smaller than the X-ray extinction distance, 13 μm.

Next to be considered is the small population of B defects, which accompanies the platelet population. Combining Woods's (1986) relation quoted in § 2, $\mu_{\mathrm{B}(1282\ \mathrm{cm}^{-1})}/\mathrm{cm}^{-1} = 20.5 \times 10^{-3} I(\mathrm{B}')/\mathrm{cm}^{-2}$, with the measured $I(\mathrm{B}')$, $30.1\ \mathrm{cm}^{-2}$, gives $\mu_{\mathrm{B}(1282\ \mathrm{cm}^{-1})} = 0.62\ \mathrm{cm}^{-1}$. The concentration of nitrogen present in B-defect form, N_B, is then derived via the relation $N_\mathrm{B} = Q_\mathrm{B} \mu_{\mathrm{B}(1282\ \mathrm{cm}^{-1})}$. Inserting $Q_\mathrm{B} = 79.4 \pm 8$ atomic ppm/cm^{-1} (Boyd *et al.* 1995) yields $N_\mathrm{B} = 49$ atomic ppm, roughly. Taking the structure of the B defect to be four substitutional nitrogen atoms tetrahedrally surrounding a vacancy (see Evans *et al.* 1995) implies a B-defect concentration of only about 12 centres per 10^6 carbon atoms. The model for the B defect poses no structural problems, but if the N–C bonds have their normal length, 0.1469 nm (Allen *et al.* 1992), and the carbon atoms concerned are undisplaced, then a rather flat NC_3 pyramid is needed, the N–C bonds then making 7.5° with (111) and the N valence angle being 118°. From this it may be concluded that the nitrogen atoms

will tend to draw together the carbon atoms with which they are bonded, resulting in some bond bending in the surrounding shell of carbon atoms. Without proper calculation, no statement can be made on the magnitude (or even sign) of the resulting ΔV_{B}, but it can be guessed to be not more than a small fraction of one carbon atomic volume. Coupled with the low concentration of B defects, it is safe to assume that their contribution to the observed dilatation of specimen A70 is insignificant. (Here, ΔV_{B} is the difference between the volume enclosing the B defect plus a few shells of surrounding carbon atoms and the corresponding volume in perfect diamond. The number of shells enclosed should be sufficient to ensure that in the outermost the only significant displacement of carbon atoms is radial and similar for all, relative to their positions in absence of the B defect.) In contrast to the situation with B defects, there is complete uncertainty regarding the dilatation contribution, if any, from the 'bonded hydrogen' defects responsible for the sharp absorption lines at 3107 cm^{-1} and 1405 cm^{-1}. The structure of these defects, whether or not they occur in clusters, and the relation between their concentration and infrared absorption strength are all unknown. In specimen A70, the integrated absorption of the strongest line, at 3107 cm^{-1}, is about 30 cm^{-2}, similar to $I(\mathrm{B}')$. However, it is reasonable to suppose that lattice parameter modification by the '3107 cm^{-1} line' defects is small compared with that produced by platelets.

For relating the properties of individual defects to the observed $\Delta a_0/a_0$, Eshelby's (1956, 1975) analysis is followed. When a pair of adjacent carbon atoms in diamond is replaced by nitrogens to form an A defect, a closed surface drawn through carbon atom centres surrounding the defect a few atomic diameters radially distant from it moves outwards to embrace a volume ΔV_{A} larger than its value before creation of the defect. All surrounding shells of diamond matrix outside this surface undergo displacement but no dilatation, in a specimen of dimensions effectively infinite, like A70. Thus the specimen volume increases by ΔV_{A}, and by $N\Delta V_{\mathrm{A}}$ when it contains N A defects, uniformly distributed. The change in $\Delta a_0/a_0$ measured by X-rays is proportional to the relative volume change of the specimen. When the crystal possesses good long range order, the volume sampled in an X-ray reflection can be taken as roughly the cube of the X-ray extinction distance, which in specimen A70 contains *ca.* 10^{11} A defects.

The action of platelets is a parting of the matrix by the sheet of abnormal platelet cells, which displace the matrix normal to the platelet plane without dilational deformation. In this case, the similar displacements relative to perfect-lattice positions undergone by many matrix cells generate the 'spike' X-ray diffuse reflections associated with platelets. Within the spikes, kinematical diffraction theory applies, whereas dynamical diffraction theory applies within the angularly sharp reflections recorded in the present experiments. The Bragg angle of the latter reflections measures the mean intercell spacing averaged over a volume roughly the cube of the extinction distance concerned, which contains of order 10^7 platelets in the case of specimen A70. Thus, the contribution to the observed $\Delta a_0/a_0$ by platelets is $\frac{1}{3}[\Delta V/V]_{\mathrm{p}}$ and is put at $[\Delta a_0/a_0]_{\mathrm{p}} = (+1.29 \pm 0.3) \times 10^{-5}$. Subtracting this 'platelet correction' from (6.1) of § 6 *a* gives the dilatation due to A defects, *ca.* 4.12×10^{-5}, disregarding possible contributions of unknown but probably small magnitude from other defects of unknown structure. A general expression of this result, bringing in infrared absorption, is: the dilatation of diamond by nitrogen impurity in A-defect form is related to the A absorption at 1282 cm^{-1}, expressed in cm^{-1}, by

$$\Delta a_0/a_0 = (0.6 \pm 0.25) \times 10^{-6}[\mu_{\mathrm{A}(1282\ \mathrm{cm}^{-1})}/\mathrm{cm}^{-1}]. \qquad (6.3)$$

The uncertainty estimate in (6.3) is believed to be realistic.

The results of Kaiser & Bond (1959), cast in similar form to (6.3), but in which $\mu_{1282\,\mathrm{cm}^{-1}}$ is total absorption at $1282\,\mathrm{cm}^{-1}$, are $\Delta a_0/a_0 = 1.46 \times 10^{-6}[\mu_{1282\,\mathrm{cm}^{-1}}/\mathrm{cm}^{-1}]$. The difference from (6.3) is attributed to very likely larger platelet populations in their specimens compared with specimen A70.

The relation between $\Delta a_0/a_0$ and A-defect nitrogen concentration is obtained from (6.3) via Q_A, applying the value adopted in § 2. This yields $\Delta a_0/a_0 = 0.036 c_{\mathrm{N(A)}}$, and the corresponding volume dilatation $\Delta V/V = 0.11 c_{\mathrm{N(A)}}$, $c_{\mathrm{N(A)}}$ being the fractional atomic concentration of A-defect nitrogen in the diamond. The numerical factor is subject to much uncertainty; if all possible errors in the chain of measurements leading to it acted in the same direction, it could be in error by about a factor of two either way. The figure $\Delta V/V = 0.11 c_{\mathrm{N(A)}}$, interpreted in terms of individual defect volumes, implies that a nitrogen atom in an A defect occupies 1.11 times the volume of a normal carbon atom in diamond (or an A defect occupies 1.11 times the volume of a pair of such atoms). This can be expressed as $[\Delta V/V]_\mathrm{A}$ per normal carbon atom replaced is 0.11.

The ratio 1.11 may be compared with that applying in the case of dispersed nitrogen singly substituting for carbon atoms. The ratio found by Lang *et al.* (1991*b*), 1.41 ± 0.06, needs to be reduced to take account of the recently revised conversion factor, Q_S, relating concentration of substitutional nitrogen, N_S, to infrared absorption at $1130\,\mathrm{cm}^{-1}$ in the relation $N_\mathrm{S} = Q_\mathrm{S}\mu_{1130\,\mathrm{cm}^{-1}}$. The increase from $Q_\mathrm{S} = 22.0 \pm 1.1$ atomic ppm per cm^{-1} absorption (Woods *et al.* 1990*b*) to $Q_\mathrm{S} = 25.0 \pm 2$ (Kiflawi *et al.* 1994) reduces the above volume ratio to 1.35 ± 0.1. Aggregation of single substitutional nitrogen into A defects increases the physical density of diamonds.

(*d*) *Comparison with computed* A*-defect structures*

Figure 8 shows the principal bond lengths and angles that change when two nitrogen atoms replace two adjacent carbon atoms to form an A defect. The reference structure (figure 8*a*) is normal diamond. The plane of the diagram contains four members of a carbon–carbon zig-zag, C1–C4, having mean direction [110]. Atom C1 and the two other carbons at the same level in (111), which are also bonded to C2, form the equilateral-triangular base of an antiprism whose top surface is formed by C4 and the other two carbons at the same height that are bonded to C3. The volume of this antiprism is adopted as the reference volume, $V(\mathrm{Ref})$, and its relative change when the A centre is formed within it gives the simplest measure of $[\Delta V/V]_\mathrm{A}$. Certainly, if there were no change from $V(\mathrm{Ref})$, it could safely be concluded that $[\Delta V/V]_\mathrm{A} = 0$, but if the change were substantial this simple geometrical calculation would be inadequate. In figure 8, bond lengths are shown relative to the standard C–C bond distance, set equal to unity. Thus, in figure 8*a*, $H = \frac{5}{3}$, $R = \cos 19.47°$ and the antiprism volume, $V(\mathrm{Ref})$, equal to $1.299 H R^2$, is here $1.299 \times 1.481 = 1.924$ volume units.

Figure 8*b* shows the A-defect structure described by Briddon (1990) and Jones *et al.* (1992). The latter paper gives the N1–N2 bond distance, 2.14 Å, and the N1–C1 (and N2–C4) bond distance, 1.46 Å. (The standard C–C bond distance used was 1.5367 Å.) Briddon (1990) gives the N–N–C angle, 99°. In figure 8*b*, $H = 1.690$ and $R = 0.9384$ (the last digits being not significant). Hence for this structure, here termed Br1, $V(\mathrm{Br1})/V(\mathrm{Ref}) = 1.00$. Such a value is incompatible with the experimental findings, which, despite their imprecision, quite definitely specify a significant positive $\Delta a_0/a_0$ due to A defects.

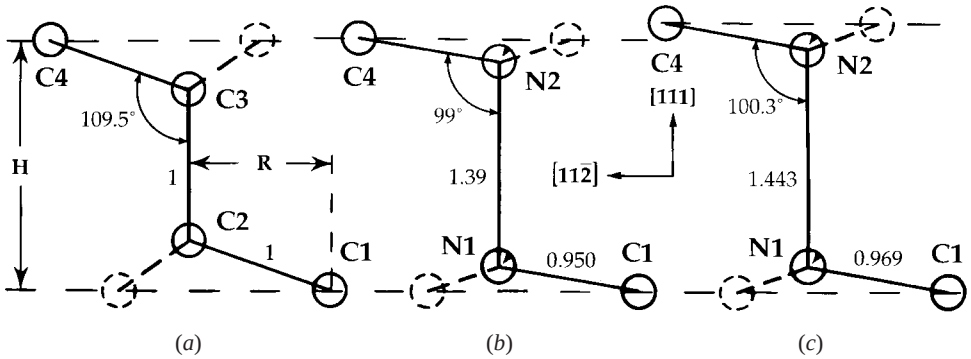

Figure 8. Comparison of computed A-defect structures with normal diamond structure. Full circles denote atoms in plane of drawing, which is ($\bar{1}$10). Interrupted circles denote carbon atoms out of plane of drawing, lying in (111) planes normal to (11$\bar{2}$). Normal C–C distance taken as unity. (*a*) Normal diamond, in which the reference volume, V(Ref) is defined (see text). (*b*) A-defect structure Br1, V(Br1)/V(Ref) = 1.00. (*c*) A-defect structure Br2, V(Br2)/V(Ref) = 1.10.

However, a new picture is presented in figure 8*c*. The authors are grateful to Dr Patrick Briddon for recalculating the bond distances and angles in the A-defect model, using a larger cluster (176 atoms instead of 86) and other refinements in technique. In the newly computed structure (Br2), the N1–N2 distance is 2.217 Å, N1–C1 is 1.489 Å and the N–N–C angle is 100.3°. These give $H = 1.789$ and $R = 0.9533$, from which V(Br2)/V(Ref) = 1.10. Since this ratio does not require substantial distortion of the immediately surrounding matrix, it can be directly interpreted as giving $[\Delta V/V]_{\mathrm{A}} = 0.10$. The close agreement of this new structure with the experimentally determined $[\Delta V/V]_{\mathrm{A}} = 0.11$ is encouraging, though the large uncertainty in the latter value must be kept in mind.

7. Concluding remarks

Experience suggests that a precision of about one part in 10^5 represents the practicably achievable limit in the lattice parameter measurement method employed. To achieve this limit with specimens in which $\varepsilon'\mu t$ is greater than about 0.2, say, requires a correction for the shift of deficiency line peak angle from that given by Bragg's Law (applied setting $\lambda = \lambda_{\mathrm{cryst}}$), assuming also that high-angle reflections from planes not steeply inclined to the X-ray entrance surface are being recorded. Here ε' is not the theoretical value, ε, but that appropriate to the perfection of the crystal under investigation; ε' must be found by matching observed with computed deficiency line profiles or by auxiliary experiments such as rocking curve analysis by double-crystal diffractometry.

The lattice parameter measured for pure, perfect diamond at room temperature, $a_0 = 0.356710$ nm, is the same as that previously recommended on the basis of a revision of results published by other workers (Lang 1994*b*), and adds some weight to that recommendation.

Specimens exhibiting B′ and B absorption spectral components as weak or weaker relative to the A component than is the case in specimen A70 are rare to very rare. Those with I(B′) a few times higher relative to their A component are fairly common. The latter still appear dominantly type IaA spectrally, and probably would have been accorded this description 40 years ago before development of precise techniques for

decomposing absorption spectra into A, B and other components. (It is possible to read into Kaiser & Bond's account of their experiments that they subtracted from their raw measurement an allowance for a B-absorption contribution when need for such correction was evident.) In fact, it only requires $I(\mathrm{B}')$ to be 3.6 times that observed in specimen A70 to bring the observed $\Delta a_0/a_0$ given in (6.1) up to a value in accord with Kaiser & Bond's finding $\Delta a_0/a_0 = 1.46\times10^{-6}[\mu_{1282\ \mathrm{cm}^{-1}}/\mathrm{cm}^{-1}]$ cited in § 6 *c*. Evidence exists that platelets are the dominating dilatation-producing defects in natural type IaA/B diamonds that are 'regular' as defined by Woods (1986). Preliminary experiments on a natural mixed-habit-growth diamond in which the {111} growth sectors were exceptionally rich in platelets, whereas the cuboid growth sectors were weaker in A-absorption and much weaker in $I(\mathrm{B}')$, found the lattice parameter excess in {111} sectors to be significantly greater than that in cuboid sectors compared with the increase expected on the basis of the greater A-absorption alone in {111} sectors, using Kaiser & Bond's relation quoted above (Lang *et al.* 1986, unpublished research). Applying the figures that emerge from the present analysis, the volume increments produced by insertion into perfect diamond of platelets, A defects and B defects can be stated. Expressing all as volumes of diamond carbon atoms per defect, the values are, for a single platelet cell (base area a normal diamond FCC a_0^2), 3.2; for a single A defect, *ca.* 0.12 (given by $(8/a_0^3)\Delta V(\mathrm{Ref})$); and for a B defect probably zero.

We thank Professor G. Davies (King's College London) and Dr C. M. Welbourn (DTC Research Centre, Maidenhead) for the loan of specimens, Dr D. Fisher and Dr P. M. Spear (DTC Research Centre, Maidenhead) for valuable help in infrared absorption measurements, and Dr R. Jones (University of Exeter) and Dr P. R. Briddon (University of Newcastle) for discussion and data on the A-defect structure. G.P. thanks De Beers Industrial Diamond Division (Pty) Ltd for financial support.

References

Allen, F. H., Kennard, O., Watson, D. G., Brammer, L., Orpen, A. G. & Taylor, R. 1992 *International tables for crystallography* (ed. A. J. C. Wilson), vol. C , ch. 9.5, pp. 685–706. Dordrecht: Kluwer.

Boyd, S. R., Kiflawi, I. & Woods, G. S. 1994 The relationship between infrared absorption and the A defect concentration in diamond. *Phil. Mag.* B **69**, 1149–1153.

Boyd, S. R., Kiflawi, I. & Woods, G. S. 1995 Infrared absorption by the B nitrogen aggregate in diamond. *Phil. Mag.* B **72**, 351–361.

Briddon, P. R. 1990 Defects in solids: an *ab initio* study. Ph.D. thesis, University of Exeter, UK.

Burns, R. C., Cvetkovic, V., Dodge, C. N., Evans, D. J. F., Rooney, M.-L. T., Spear, P. M. & Welbourn, C. M. 1990 Growth-sector dependence of optical features in large synthetic diamonds. *J. Crys. Growth* **104**, 257–279.

Bursill, L. A., Hutchison, J. L., Sumida, N. & Lang, A. R. 1981 Measurements of diamond lattice displacement by platelet defects with electron microscopic moiré patterns. *Nature* **292**, 518–520.

Cherns, D., Kaneko, K., Hovsepian, A. & Lang, A. R. 1997 Measurement of the lattice displacement across {100} platelets in diamond by large angle convergent beam electron diffraction. *Phil. Mag.* A **75**, 1553–1566.

Clackson, S. G., Moore, M., Walmsley, J. C. & Woods, G. S. 1990 The relationship between platelet size and the frequency of the B′ infrared absorption peak in type Ia diamond. *Phil. Mag.* B **62**, 115–128.

Cohen, E. R. & Taylor, B. N. 1986 *The 1986 adjustment of the fundamental physical constants, CODATA Bulletin 63.* Elmsford, NY: Pergamon.

Davies, G. 1976 The A aggregate in diamond—its symmetry and possible structure. *J. Phys.* C **9**, L537–L542.

Davies, G. 1977 The optical properties of diamond. In *Chemistry and physics of carbon* (ed. P. L. Walker & P. A. Thrower) vol. 13, pp. 1–143. New York: Marcel Dekker.

Deutsch, M., Hölzer, G., Härtwig, J., Wolf, J., Fritsch, M. & Förster, E. 1995 K_α and K_β X-ray emission spectra of copper. *Phys. Rev.* A **51**, 283–296.

Eshelby, J. D. 1956 The continuum theory of lattice defects. *Solid State Phys.* **3**, 79–144.

Eshelby, J. D. 1975 Point defects. In *The physics of metals 2. Defects* (ed. P. B. Hirsch), pp. 1–42. Cambridge University Press.

Evans, T., Kiflawi, I., Luyten, W., van Tendeloo, G. & Woods, G. S. 1995 Conversion of platelets into dislocation loops and voidite formation in type IaB diamonds. *Proc. R. Soc. Lond.* A **449**, 295–313.

Härtwig, J., Grosswig, S., Becker, P. & Windisch, D. 1991 Remeasurement of the CuKα_1 emission X-ray wavelength in the Metrical System (present stage). *Phys. Status Solidi* A **125**, 79–89.

Hildebrandt, G., Stephenson, J. D. & Wagenfeld, H. 1975 Photoelectric atomic absorption cross sections for elements Z = 6 to 54 in the medium energy X-ray range (5 to 25 keV). I. *Z. Naturf.* **30a**, 697–707.

Holloway, H., Hass, K. C., Tamor, M. A., Anthony, T. R. & Banholzer, W. G. 1991 Isotopic dependence of the lattice constant of diamond. *Phys. Rev.* B **44**, 7123–7126. (Erratum 1992 *Phys. Rev.* B **45**, 6353).

James, R. W. 1954 *The optical principles of the diffraction of X-rays.* London: G. Bell and Sons.

James, R. W. 1963 The dynamical theory of X-ray diffraction. *Solid State Phys.* **15**, 53–219.

Jones, R., Briddon, P. R. & Öberg, S. 1992 First-principles theory of nitrogen aggregates in diamond. *Phil. Mag. Lett.* **66**, 67–74.

Kaiser, W. & Bond, W. L. 1959 Nitrogen, a major impurity in common type 1 diamond. *Phys. Rev.* **115**, 857–863.

Kiflawi, I., Mayer, A. E., Spear, P. M., van Wyk, J. A. & Woods, G. S. 1994 Infrared absorption by the single nitrogen and A defect centres in diamond. *Phil. Mag.* B **69**, 1141–1147.

Kossel, W. 1937 Röntgeninterferenzen aus Gitterquellen. *Ergebnisse der Exakten Naturwiss* **16**, 295–352.

Lang, A. R. 1974 On the growth-sectorial dependence of defects in natural diamonds. *Proc. R. Soc. Lond.* A **340**, 233–248.

Lang, A. R. 1993 Dilatation, density and nitrogen content in type IaA diamond. *J. Phys.: Appl. Phys.* D **26**, 2239–2244.

Lang, A. R. 1994*a* X-ray topographic and optical imaging studies of synthetic diamonds. *J. Appl. Crystallogr.* **27**, 988–1001.

Lang, A. R. 1994*b* Lattice parameter determinations in diamond—an overview. In *Properties and growth of diamond* (ed. G. Davies), pp. 106–110. London: IEEE.

Lang, A. R. 1995 Exploitation of n-beam dynamical effects in pseudo-Kossel diffraction patterns of nearly perfect crystals. *J. Phys.: Appl. Phys.* D **28**, A1–A7.

Lang, A. R. & Meaden, G. 1991 Complementary orientation-dependent disributions of 1.40 eV and 2.56 eV cathodoluminescence on vicinals on {111} in synthetic diamonds. *J. Crystal Growth* **108**, 53–62.

Lang, A. R. & Pang, G. 1995 A possible new route to precise lattice parameter measurement of perfect crystals using the divergent beam method. *J. Appl. Crystallogr.* **28**, 61–64.

Lang, A. R., Kowalski, G., Makepeace, A. P. W. & Moore, J. 1991*a* On long-range lattice perfection in type Ia diamond. *Phil. Mag.* A **64**, 543–560.

Lang, A. R., Moore, M., Makepeace, A. P. W., Wierzchowski, W. & Welbourn, C. M. 1991*b* On the dilatation of synthetic type Ib diamond by substitutional nitrogen impurity. *Phil. Trans. R. Soc. Lond.* A **337**, 497–520.

Lang, A. R., Pang, G. & Makepeace, A. P. W. 1996 Applications of synchrotron radiation to defect characterization and Pendellösung fringe spacing measurement in a natural diamond. *J. Synchrotron Radiat.* **3**, 163–172.

Lonsdale, K. 1947 Divergent-beam X-ray photography of crystals. *Phil. Trans. R. Soc. Lond.* A **240**, 219–250.

Reeber, R. R. & Wang, K. 1996 Thermal expansion, molar volume and specific heat of diamond from 0 to 3000 K. *J. Electronic Mater.* **25**, 63–67.

Reid, J. S. & Pirie, J. D. 1980 Dynamic deformation and the Debye–Waller factors for silicon-like crystals. *Acta. Crystallogr.* A **36**, 957–965.

Runciman, W. A. & Carter, T. 1971 High resolution infra-red spectra of diamonds. *Solid State Commun.* **9**, 315–317.

Sumida, N. & Lang, A. R. 1988 On the measurement of population density and size of platelets in type 1a diamond and its implications for platelet structure models. *Proc. R. Soc. Lond.* A **419**, 235–257.

Takama, T., Tsuchiya, K., Kobayashi, K. & Sato, S. 1990 Measurement of the structure factors of diamond. *Acta Crystallogr.* A **46**, 514–517.

von Laue, M. 1960 *Röntgenstrahlinterferenzen*. Frankfurt: Akad.

Welbourn, C. M., Rooney, M.-L. T. & Evans, D. J. F. 1989 A study of diamonds of cube and cube-related shape from the Jwaneng Mine. *J. Crystal Growth* **94**, 229–252.

Woods, G. S. 1986 Platelets and the infrared absorption of type Ia diamonds. *Proc. R. Soc. Lond.* A **407**, 219–238.

Woods, G. S. & Collins, A. T. 1983 Infrared absorption spectra of hydrogen complexes in type I diamonds. *J. Phys. Chem. Solids* **44**, 471–475.

Woods, G. S., Purser, G. C., Mtimkulu, A. S. S. & Collins, A. T. 1990*a* The nitrogen content of type Ia natural diamonds. *J. Phys. Chem. Solids* **51**, 1191–1197.

Woods, G. S., van Wyk, J. A. & Collins, A. T. 1990*b* The nitrogen content of type Ib synthetic diamond. *Phil. Mag.* B **62**, 589–595.

PHILOSOPHICAL TRANSACTIONS OF THE ROYAL SOCIETY A MATHEMATICAL, PHYSICAL & ENGINEERING SCIENCES

PHILOSOPHICAL TRANSACTIONS OF THE ROYAL SOCIETY A MATHEMATICAL, PHYSICAL & ENGINEERING SCIENCES